scientific reports

OPEN

Glucocorticoids induce femoral head necrosis in rats through the HIF-1α/VEGF signaling pathway

HaoXu Tang[1,2], Lingli Yuan[2✉], ZhiYuan Xu[3], GuiFen Jiang[4], YingJie Liang[2], Ce Li[2], PengLin Ding[2] & MinLong Qian[2]

Glucocorticoid-induced osteoblast dysfunction is the primary cause of steroid-induced osteonecrosis of the femoral head (SONFH). However, the specific underlying biological mechanisms of glucocorticoids' effect on osteoblasts remain undetermined. Recently, the role of hypoxia-inducible factor 1-alpha (HIF-1α)/vascular endothelial growth factor (VEGF) signaling pathway in modulating bone formation has been studied. This study aimed to investigate the association and mechanism of the HIF-1α/ VEGF signaling pathway in glucocorticoid-induced osteogenesis suppression in MC3T3-E1 cells. This study performed CCK8 and live/dead staining assays by stimulating MC3T3-E1 cells with varying dexamethasone (DEX) doses to elucidate its influence on cell proliferation and activity. Furthermore, Western blotting was carried out to investigate the expression of HIF-1α, runt-related transcription factor 2 (RUNX2), VEGF, osteopontin (OPN), and alkaline phosphatase (ALP) proteins to identify the optimal DEX concentration for simulating steroid-induced osteonecrosis cell models. Moreover, the osteogenic differentiation of cells was assessed by transfecting them with control or HIF-1α overexpression lentiviral vectors. Similarly, in vivo, hematoxylin and eosin staining, immunohistochemical staining, and micro-computed tomography were performed to validate in vitro results in the SONFH rat model. In vitro analyses revealed that a 10^{-6} M concentration of DEX significantly suppressed cell viability and osteogenesis by decreasing HIF-1α and VEGF levels. Furthermore, HIF-1α upregulation increased osteogenic activity and VEGF expression in MC3T3-E1 cells. However, the HIF-1α antagonist 3-(5'-hydroxymethyl-2'-furyl) -1-benzylindazole (YC-1) indicated opposite effects in DEX-treated MC3T3-E1 cells. Moreover, SONFH femoral heads had reduced bone density, bone tissue content, and femoral head integrity, as well as increased bone cell lacunae, while decreased HIF-1α, OPN, VEGF, and ALP levels in bone tissue compared to normal rats. This study indicated that DEX suppresses osteoblast differentiation *via* the HIF-1α/VEGF pathway, thus promoting SONFH.

Keywords Steroid-induced osteonecrosis of the femoral head, HIF-1α, VEGF, Osteoblasts, Osteogenic differentiation

Abbreviations

SONFH	Steroid-induced osteonecrosis of the femoral head
HIF-1α	Hypoxia-inducible factor 1-alpha
VEGF	Vascular endothelial growth factor
DEX	Dexamethasone
OPN	Osteopontin
RUNX2	Runt-related transcription factor 2
ALP	alkaline phosphatase
OCN	Osteocalcin
Micro CT	Micro-computed tomography
HE	Hematoxylin and eosin
YC-1	3-(5'-hydroxymethyl-2'-furyl)-1-benzylindazole
BMSCs	Bone marrow mesenchymal stem cells

[1]Department, Bengbu Medical University, Anhui, China. [2]Department of the Second, Affiliated Hospital of Bengbu Medical University, Anhui, China. [3]Department of the Bozhou People's Hospital, Bengbu, Anhui, China. [4]Department of Pathology, The Sixth Affiliated Hospital, School of Medicine, South China University of Technology, Guangdong, China. ✉email: 2129798218@qq.com

BMD	Bone mineral density
BV/TV	Bone volume per tissue volume
Tb.N	Trabecular number
Tb.Th	Trabecular thickness
Tb.Sp	Trabecular spacing
Tb.Pf	Trabecular pattern of bone due to factor

Glucocorticoids are broadly applied clinically because of their effectiveness against various conditions, such as autoimmune diseases, inflammatory disorders, and allergies[1–3]. However, glucocorticoids have significant adverse effects, including osteocyte apoptosis and osteonecrosis[4–6], and are the primary risk factor for non-traumatic femoral head osteonecrosis[7,8]. Prolonged or high-dose glucocorticoid use causes steroid-induced osteonecrosis of the femoral head (SONFH)[9], which is an intractable chronic condition that often leads to irreversible joint surface collapse and consequent joint dysfunction[10]. The current therapeutic options are limited, and advanced cases are typically managed through surgery[11], including intramedullary decompression[12] or osteotomy[13]. Furthermore, cell therapy has also been employed[14]; however, the prognosis remains poor[15]. The etiology of SONFH is incompletely understood, and there are limited effective clinical interventions. Therefore, it is essential to investigate the molecular mechanisms underlying SONFH to develop prevention and management strategies.

Previous literature has associated hypoxia with skeletal metabolic disorders, and both pathological and environmental hypoxia impact bone health. Adaptation to hypoxia is a key issue during normal cell development and differentiation, as well as in pathological conditions such as ischemia[16]. Hypoxia-inducible factor 1 (HIF-1) is a crucial transcriptional regulator for the cellular hypoxia response. It comprises HIF-1β and HIF-1α subunits that bind hypoxia response elements to modulate target gene expression, gene transcription[17], cell proliferation, differentiation[18], migration[19], and homing[20,21], eliciting specific biological effects. During normoxic conditions, HIF-1α is degraded, however, it remains stable under hypoxia[22,23]. Furthermore, the expression of HIF-1α is crucial for preventing bone metabolic diseases during pathological state[24,25]. It has been observed that under reduced oxygen tension, osteoblasts and related cells stabilize HIF-1α expression, modulating angiogenic and osteogenic gene expression[26]. Moreover, HIF-1α overexpressing mice have indicated increased bone volume and osteoblast counts[25], suggesting that HIF-1 has a significant role in osteogenesis and bone repair[27,28]. However, HIF-1α's effect on glucocorticoid-mediated osteoblast osteogenic suppression remains elusive.

Studies have observed a significant spatiotemporal correlation between angiogenesis and osteogenesis in bone development and regeneration processes. Neovascularization is essential for bone regeneration[29]. During a hypoxic state, the HIF-1α/VEGF pathway has been found to induce osteogenic differentiation of bone marrow mesenchymal stem cells (BMSCs) and promote vascular endothelial cells' proliferation, migration, and angiogenesis[30,31]. In hypoxic or ischemic cells, HIF-1α increases the expression of VEGF[32], which is essential for angiogenesis and vascular remodeling. Moreover, HIF-1α activated VEGF identifies bone-specific endothelial cells and promotes bone angiogenesis. Therefore, investigating VEGF is crucial for elucidating the complex pathogenesis of SONFH.

This research study aims to elucidate the role of the HIF-1α/VEGF pathway in dexamethasone (DEX)-treated osteoblasts in vitro analyses. Based on these analyses, an in vivo SONFH model was developed to assess the association of glucocorticoids with SONFH pathogenesis. The findings will offer novel evidence for the clinical management of SONFH.

Materials and methods
Cell culture and osteogenic differentiation
The MC3T3-E1 cell line was procured from iCell Bioscience Inc (Shanghai, China) and grown in α-MEM medium (Gibco, USA) augmented with 1% penicillin/streptomycin (Biosharp, China) and 10% FBS (Priscilla, China) at 37 °C in 5% CO_2. The medium was refreshed every 2 days. Upon 80% confluency, osteogenic differentiation was induced by replacing the standard medium with an osteogenic-specific solution. This specialized medium was prepared with α-MEM, 50 μg/mL of L-ascorbic acid, and 10 mM of Sodium β-glycerophosphate (Sigma-Aldrich, USA).

Dexamethasone treatment
MC3T3-E1 cells were grown and divided into two groups. Group 1 cells were grown in the osteogenic medium and treated with different DEX (Sigma-Aldrich, USA) doses. Cell proliferation rate was evaluated on the 1st, 2nd, and 3rd day *via* the CCK-8 test (Biosharp, China). Group 2 cells were grown in a medium lacking DEX or containing 10^{-6} M DEX in the presence or absence of YC-1 (10 μM) for 7 days.

Cell proliferation and viability assessment
The proliferation of DEX-treated MC3T3-E1 cells was assessed *via* the CCK-8 test. Briefly, cells (5000/well) were plated in 96-well dishes and grown with or without DEX for 3 days. Cell proliferation was evaluated by measuring absorbance *via* a microplate reader at 450 nm. After 34 h, cell viability was determined using the Live-Dead Cell Staining Kit, where green dye-stained live cells while red dye-stained dead cells.

Transfection assay
Lentiviral plasmids overexpressing HIF-1α (HIF-1α-OE) and negative control (OE-Ctrl) groups were established by GeneChem (Shanghai, China) and transfected in cells per the kit's guide. The transfected cells were named HIF-1α-OE or Ctrl-OE, while the untransfected cells were labeled Ctrl. After 72 h of transfection, stable transgenic cells were selected using puromycin. Target proteins and gene expressions were validated by WB and qRT-PCR, respectively.

ALP staining

Following osteogenic induction, the culture medium was aspirated, the cells were rinsed with PBS (Priscilla, China) 3 times, preserved for 30 min in 4% paraformaldehyde, and subjected to ALP staining *via* the BCIP/NBT kit (Beyotime Biotechnology, China). Cells were then incubated in the dark for 30 min at 37 °C, and the reaction was stopped using deionized water. Then, microscopic analysis was performed.

Alizarin red staining (ARS)

After 21 days in the osteogenic medium in a 6-well plate, cells were fixed using 4% paraformaldehyde for 30 min, rinsed 2 times with PBS, and stained with Alizarin Red working solution (Cyagen Biosciences, China) for 30 min, followed by two deionized water rinses. The intensity of ARS was observed under an optical microscope.

Western Blotting

Whole protein was harvested from the MC3T3-E1 cells using RIPA buffer comprising protease inhibitors (Beyotime Biotechnology, China). Proteins in the supernatant were quantified *via* the BCA assay kit (Epizyme Biotech, China). Thirty micrograms of protein per sample were subjected to 7.5% or 10% SDS-PAGE and electrotransferred onto PVDF membranes (0.45 μm; Millipore), which were then sealed with a closure buffer (Epizyme Biotech, China) and treated overnight with HIF-1α (1:1000, Abcam, UK), RUNX2 (1:1000, Affinity, China), VEGF (1:1000, HUABIO, China), OPN (1:1000, Abcam, UK), ALP (1:1000, Affinity, China), and anti-β-actin (1:5000, Affinity, China) antibodies at 4 °C. After TBST washing, the membrane was probed for 2 h with the secondary antibody (1:5000, Affinity, China) and washed thrice with TBST. Protein blots were imaged using an enhanced ECL chemiluminescent substrate kit (Millipore, USA). ImageJ software was employed to perform quantitative analysis of protein blots. The gray value of the target protein was divided by the gray value of the reference protein β-actin for normalization.

Quantitative real-time qPCR

For whole RNA collection, TRIZOL reagent (Invitrogen, USA) was employed. cDNA was prepared *via* reverse transcription per the protocol of the HiScript III RT SuperMix for qPCR (+ gDNA wiper) (Vazyme, China). The ChamQ Universal SYBR qPCR Master Mix (Vazyme, China) was employed for qRT-PCR, and the cycling conditions were 30 s at 95 °C, 5 s at 95 °C, and 30 s at 60 °C for 40 cycles. A melting curve was plotted from 65 °C to 95 °C. In this study, the 2-ΔΔCT method was utilized for assessing the fold changes in the target mRNA expression, which were normalized to glyceraldehyde-3-phosphate dehydrogenase (GAPDH). The primers employed for this analysis (Sangon Biotech, Shanghai, China) are as follows:

HIF-1α:
Forward: 5′-gagatgaaggcacagatggact-3′.
Reverse: 5′-aatgtaaaccatgtcgccgt-3′.
GAPDH.
Forward: 5′-ggttgtctcctgcgacttca-3′.
Reverse: 5′-tggtccagggtttcttactcc-3′.
Animal models and group assignments.

Sprague-Dawley (SD) rats ($n = 20$, male, weight $= 200 \pm 20$ g) were procured from Wukon Biotechnology in China and maintained in a controlled, pathogen-free facility, at 26 °C, 55% humidity, and 12-hour light/dark cycle, with ad libitum access to chow and water. After a week of acclimatization, the rats were randomly categorized into the model and normal control (Ctrl) groups ($n = 10$/group). The glucocorticoid-induced SONFH model was established as per a previous study[33]. The model rats were intraperitoneally administered 40 μg/kg of lipopolysaccharide (LPS, Sigma, USA) once daily for four consecutive days and intramuscularly injected with 60 mg/kg of methylprednisolone (MPS, Pfizer, USA) once daily. The Ctrl group was administered the same volume of saline solution and kept under the same conditions. All samples were collected 6 weeks post-initial MPS injection. All animal studies were authorized by the Ethics Committee of Bengbu Medical University [Number: (2022) No. 159] and followed their established protocols. All experimental procedures were conducted following the ARRIVE guidelines.

Serum ALP

The rats were anesthetized by intraperitoneal injection of 2% sodium pentobarbital (40 mg/kg), and blood was collected from the abdominal aorta, leading to their death from shock. Blood samples were collected from anesthetized SD rats using serum separator tubes, which were kept at room temperature for 2 h and then centrifuged for 20 min at 4 °C and 3000 rpm to collect serum. An ALP/AKP assay kit (Bioengineering Institute, Nanjing, China) was used to assess serum ALP levels, per the kit's guide. Briefly, serum samples were treated with the reagent solution for 15 min in a water bath at 37 °C. Then, absorbance was read *via* a microplate reader (Bio-Tek Instruments, USA) at 520 nm. One Gold's unit (U) was defined as the amount of serum that produces 1 mg of phenol when reacted with the substrate at 37 °C for 15 min in a 100 mL sample.

MicroCT analysis

The morphological changes of the rat's skeleton were assessed *via* Micro-CT of the femoral heads of each rat with a 9-micrometer voxel resolution. The acquired two-dimensional images were then imported into CTan software for analysis. The region of interest (ROI) was selected in the area of subchondral bone of the femoral head based on the literature[34] and key bone quality parameters analysis including trabecular bone number (Tb.N), bone volume (BV), trabecular bone pattern factor (Tb.Pf), bone volume fraction (BV/TV), trabecular bone thickness (Tb.Th), bone mineral density (BMD), and trabecular bone separation (Tb.Sp).

Hematoxylin-eosin (HE) staining and immunohistochemical analysis

Rat femoral heads were preserved in formalin for 48 h, decalcified using EDTA solution for over 4 weeks, submerged in paraffin, sliced (5 µm thick), and stained with HE. The HE staining was performed to assess the trabecular bone structure and osteocyte lacunae.

For immunohistochemical assays, sections were dewaxed, subjected to antigen retrieval, and treated with anti-HIF-1α (1:200, Abcam), anti-CD31 (1:2000, Abcam), anti-ALP (1:200, Abcam), anti-OPN (1:2000, Abcam), and anti-VEGF (1:200, Abcam) primary antibodies, followed by incubation with corresponding secondary antibodies. Then, the sections were dyed with 3'-diaminobenzidine and counterstained with hematoxylin. After imaging, the ratio of the positive cell area to the respective total area in each of the three fields of view in every section was measured *via* the ImageJ software. Subsequently, the positivity rate (%) was calculated: (positive cell area/total area) × 100.

Statistical analysis

GraphPad Prism 8 was employed for the statistical assessments and data visualization. All the data were depicted as means ± standard deviation. Data that satisfied the tests for normal distribution and homogeneity of variance were analyzed using a t-test to assess differences between two groups, while comparisons among multiple groups were performed using one-way analysis of variance (ANOVA) followed by Tukey's post hoc test. Differences were considered statistically significant at $p < 0.05$.

Results

DEX inhibits MC3T3-E1 cell proliferation and decreases cell viability

To assess DEX's impacts on osteoblast proliferation, MC3T3-E1 cells were stimulated with DEX (10^{-8}-10^{-6} M doses) for 1, 2, and 3 days. CCK-8 assays revealed that DEX reduced osteoblast viability dose-dependently. Compared to the Ctrl group, the 10^{-6} M DEX-treated cells had markedly reduced absorbance, indicating a significant suppression of proliferation. Furthermore, the response of 10^{-6} M DEX-treated cells on the 1st, 2nd, and 3rd day showed that the inhibition of cell proliferation was dose- and time-dependent (Fig. 1A). Live-dead cell staining assays showed that the number of dead cells increased with increasing DEX concentrations, which was visually confirmed under an optical microscope (Fig. 1B and C).

DEX downregulates the expression of proteins related to the HIF-1α/VEGF signaling pathway and osteogenesis

To investigate HIF-1α expression in glucocorticoid-mediated osteogenic suppression, MC3T3-E1 cells were treated with varied DEX concentrations (10^{-8} to 10^{-6} M). The results of WB showed that the expression of the HIF-1α/VEGF pathway proteins declined with increasing DEX concentration (Fig. 2A and B). Furthermore, to assess DEX's effect on MC3T3-E1 cells' osteogenic differentiation, WB was carried out to evaluate the protein levels of osteogenic markers, including RUNX2, ALP, and OPN.

The data revealed that after DEX treatment, the ALP, RUNX2, and OPN levels in MC3T3-E1 cells reduced dose-dependently (Fig. 2A and C), suggesting that DEX can inhibit the ability and function of osteoblasts. Based on these findings, MC3T3-E1 cells were treated with 10^{-6} M DEX to simulate hormone-induced femoral head osteonecrosis in vitro in the subsequent experiments. Furthermore, ALP staining after 7 days (Figs. 2D and F) and ARS after 21 days (Figs. 2E and G) of osteogenic induction validated that DEX significantly inhibited the MC3T3-E1 cell's osteogenic differentiation ability. Therefore, it was hypothesized that the HIF-1α/VEGF pathway might be pivotal for MC3T3-E1 cells' osteogenic differentiation.

Upregulation of HIF-1α attenuates the suppressive effects of DEX on the osteogenic functions of MC3T3-E1 cells.

To validate the above hypothesis, a lentiviral-mediated HIF-1α overexpression (OE) system was established and transfected into MC3T3-E1 cells. The HIF-1α-OE efficiency was confirmed by qRT-PCR and WB, which indicated that HIF-1α-OE substantially increased HIF-1α expression compared to the control and OE-Ctrl groups (Fig. 3A-C). The transfected MC3T3-E1's osteogenic differentiation potential was evaluated using ALS and ALP staining. The data showed that DEX-treated MC3T3-E1 cells had markedly increased HIF-1α expression, which was validated by the increased number of purple-stained cells and red calcium nodules, indicating improved osteogenic function (Fig. 4). The WB analysis results further confirmed these observations, revealing a marked upregulation of osteogenic markers, RUNX2, ALP, and OPN, in the HIF-1α-OE group related to the DEX-treated group (Fig. 3D and F). Further, in DEX-induced MC3T3-E1 cells, HIF-1α-OE positively modulated VEGF expression (Fig. 3D and E), indicating the activation of the HIF-1α/VEGF pathway.

### HIF-1α inhibitor reversed the protective effect of HIF-1α on DEX-induced osteogenesis Inhibition

To investigate target specificity and validate HIF-1α's role in DEX-induced osteogenesis, DEX-stimulated MC3T3-E1 cells were treated with the HIF-1α antagonist YC-1. The results of WB analysis revealed that YC-1 decreased HIF-1α and VEGF levels in DEX-treated MC3T3-E1 cells. (Fig. 5A and B), indicating that YC-1 inhibits VEGF expression. Furthermore, YC-1 promoted DEX's inhibitory effects on osteogenic markers Runx2, ALP, and OPN in MC3T3-E1 cells (Fig. 5A and C), further indicating how the HIF-1α/VEGF axis regulates DEX-induced osteogenic protein expression. Moreover, ALP staining and ARS results revealed that YC-1 substantially reduced the MC3T3-E1 cell's mineralized nodule formation and ALP activity (Fig. 6). Overall, HIF-1α-OE partially reversed the YC-1's inhibitory impact on the protein levels of HIF-1α/VEGF and osteogenic pathway; that is, HIF-1α-OE mitigated YC-1's inhibitory effects in DEX-induced MC3T3-E1 cells.
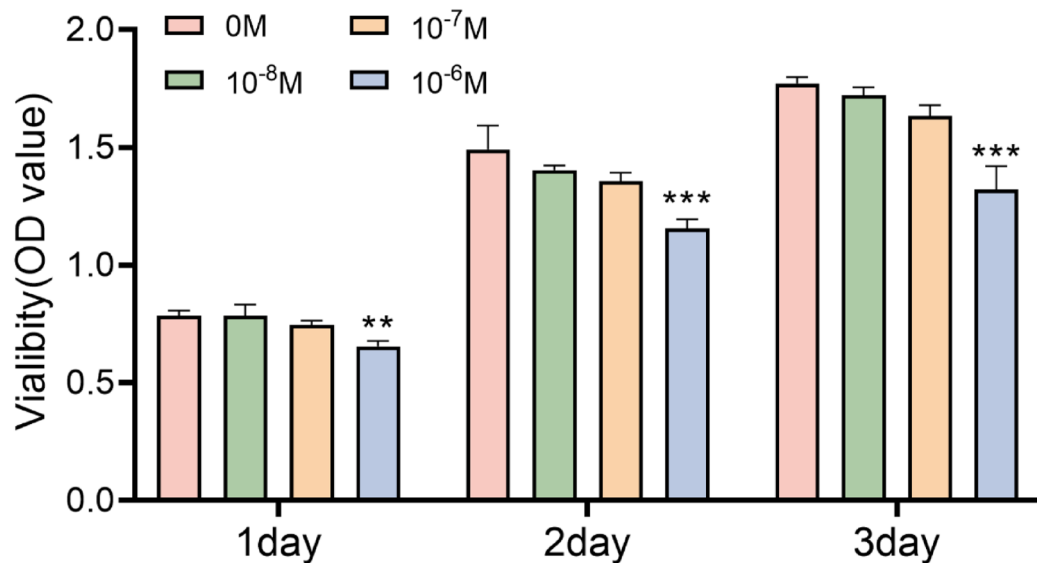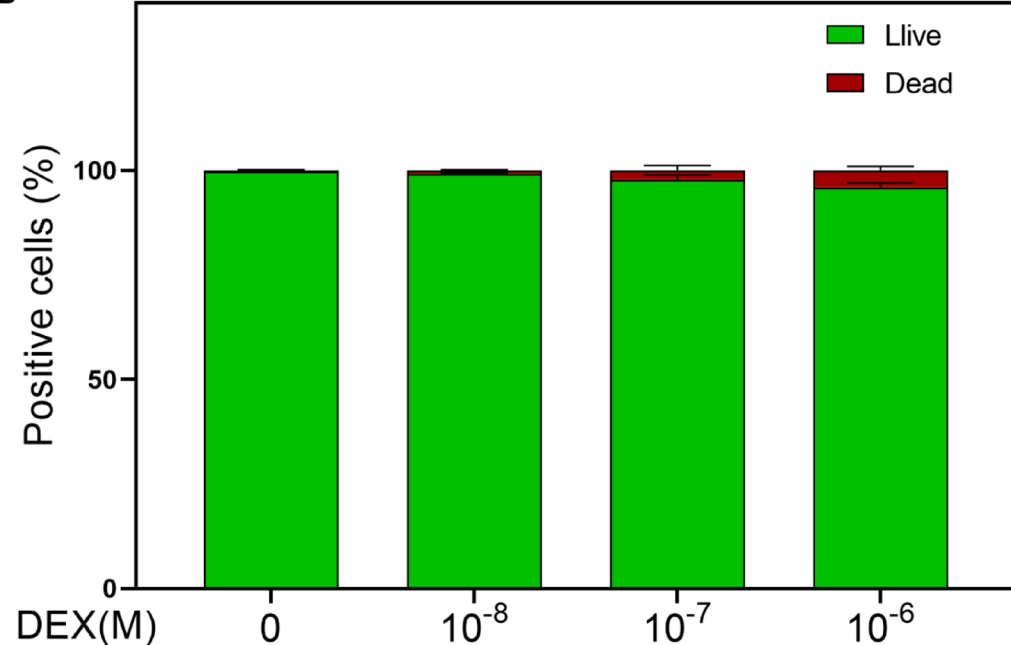
Fig. 1. The influence of various DEX concentrations on the value-added and MC3T3-E1 cell activity. **(A)** MC3T3-E1 cells were induced with different DEX levels, and the cell proliferation rate was assessed on the 1st, 2nd, and 3rd day *via* the CCK8 assay. **(B)** Quantitative analysis of the ratio of live/dead cells. **(C)** Live-dead staining analysis of MC3T3-E1 cells treated with varied DEX concentrations for 24 h. Red = dead cells, Green = live cells (Scale bar = 100 μm). *** $p < 0.001$, ** $p < 0.01$, $n = 3$ relative to control without DEX.

Rat model of steroid-induced osteonecrosis of the femoral head

To validate the successful establishment of the rat glucocorticoid-induced femoral head osteonecrosis model, Micro-CT and HE staining were carried out 6 weeks after the initial MPS injection to detect and confirm osteonecrosis. Micro-CT scanning can show trabecular bone's microstructure, mirroring tissue structure integrity and bone mass alterations. It is, therefore, the most effective approach for assessing bone tissue's microscopic structure. Here, the Micro-CT imaging and subsequent reconstruction analysis revealed that the Ctrl group rat femoral heads were structurally normal, had no signs of collapse or cavitation, and had a consistent and even distribution of trabecular bone throughout (Fig. 7A). Whereas the MPS group indicated bone mineral loss in the subchondral region of the femoral head and cavity formation, disordered trabecular bone structure, irregular arrangement, and uneven density. Furthermore, quantitative analysis of bone morphological metrics indicated

C
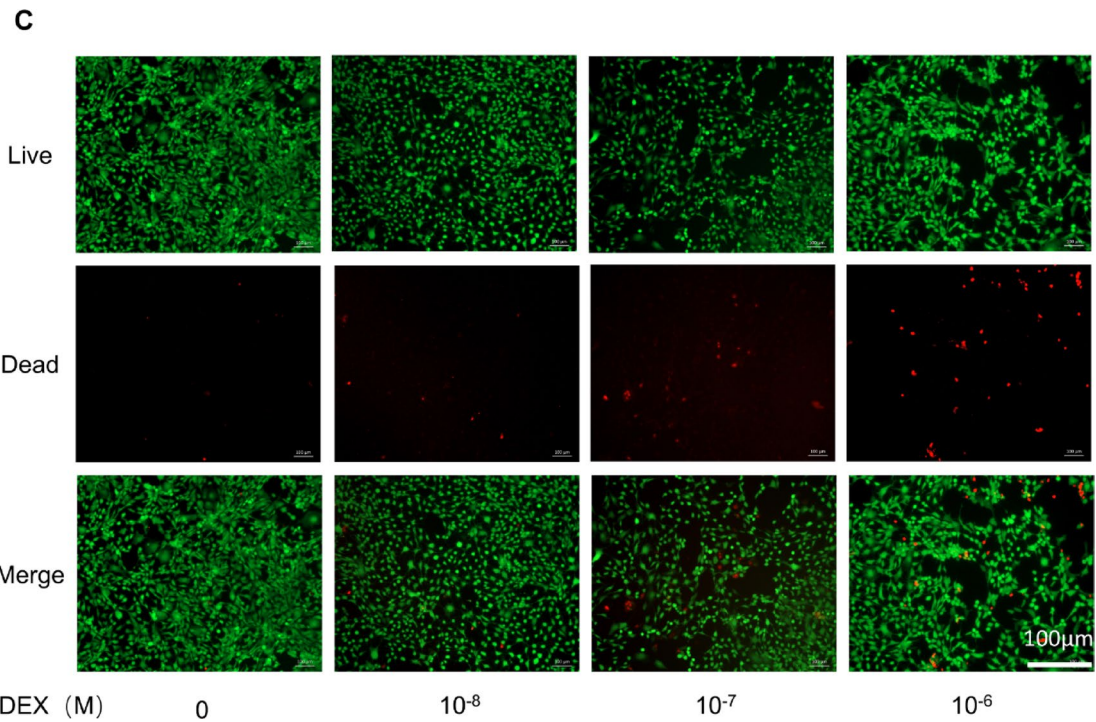
Fig. 1. (continued)

that in the hormone-treated MPS group, BMD and BV/TV were significantly inversely altered relative to the normal Ctrl group (Fig. 7B and C). Moreover, quantitative analysis of subchondral trabecular bone parameters revealed generally consistent bone morphological parameters and markedly inversed Tb.Th, and Tb.N changes in the hormone-treated MPS group compared to the Ctrl group (Fig. 7D and E). Similarly, compared with the Ctrl group, Tb.pf and Tb.Sp in the MPS group was substantially increased (Fig. 7F and G), indicating a continuous destruction of the trabecular. Consistent with the Micro-CT results (Fig. 8A), HE staining revealed that in the Ctrl group, the femoral head had orderly arranged and intact trabecular bone and rare empty osteocyte lacunae (Fig. 8B), which were surrounded by a large number of osteoblasts. Whereas in the MPS group, the femoral head indicated disorganized trabecular bone structure, nuclear shrinkage, multiple empty bone lacunae, and fat tissue infiltration. Moreover, bone mineral loss was observed in the subchondral area. Based on these results, a rat SONFH model was established for in vivo analysis.

### Serum ALP levels in rats with steroid-induced osteonecrosis of the femoral head

After 6 weeks of the initial hormone, SONFH rat's serum ALP levels were assessed, which revealed that relative to the Ctrl group, the ALP activity of MPS group rats was markedly reduced (Fig. 8C). ALP is a key biomarker of osteoblast activity, and its reduced activity may be associated with the inhibition of bone formation processes. These data suggest that glucocorticoids suppress osteoblast's activity in MPS group rats, which affects bone formation and mineralization processes, therefore decreasing ALP levels.

### Immunohistochemical analysis in rats with steroid-induced osteonecrosis of the femoral head

To further verify the potential role of HIF-1α in glucocorticoid-mediated femoral head osteonecrosis in vivo, a rat glucocorticoid-induced osteonecrosis model was developed. Immunohistochemical analysis indicated markedly reduced HIF-1α and VEGF staining in the femoral head tissue of the MPS group than the Ctrl group (Fig. 9A and B). Furthermore, the MPS rats' OPN and ALP levels were reduced compared to those of the Ctrl rats. The findings suggested that HIF-1α expression positively correlates with OPN and ALP in SONFH, further validating the crucial role of the HIF-1α/VEGF pathway in maintaining bone homeostasis and promoting bone regeneration in SONFH. VEGF is primarily responsible for initiating angiogenesis, and its expression was substantially suppressed in the SONFH rat model. This might be because glucocorticoids interfere with the signaling pathway of HIF-1α/VEGF, thus decreasing the number of blood vessels in bone tissue. To test this hypothesis, immunohistochemical staining was performed to assess angiogenesis within the femoral head, focusing on CD31, a marker of vascular endothelial cells. The results indicated a substantially reduced number of CD31-positive capillaries in the MPS group, suggesting that MPS inhibits neovascularization. Therefore, it was inferred that glucocorticoids might impede osteoblast differentiation and angiogenesis by inhibiting the HIF-1α/VEGF signaling pathway, which ultimately results in the onset of femoral head osteonecrosis.
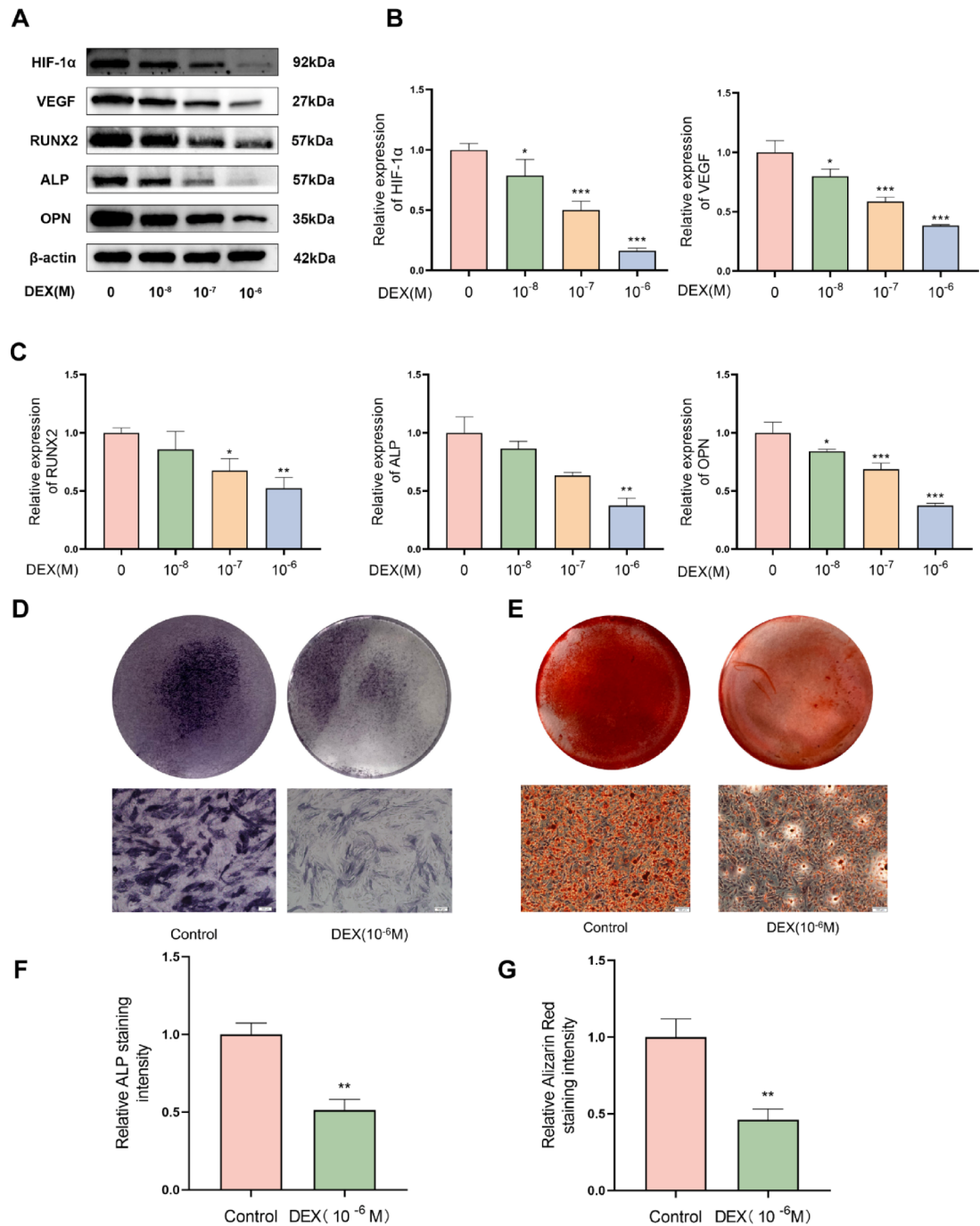
Fig. 2. Effects of varying DEX levels on HIF-1α/VEGF signaling pathway and MC3T3-E1 cells' osteogenic differentiation. (**A**) Protein levels of VEGF, Runx2, HIF-1α, ALP, and OPN in MC3T3-E1 cells treated with varying DEX doses were analyzed *via* WB. (**B**) Statistical analysis of HIF-1α and VEGF pathway protein expression in MC3T3-E1 cells treated with varying DEX concentrations. (**C**) Statistical analysis of Runx2, ALP, and OPN osteogenic marker protein expression in MC3T3-E1 cells treated with varying DEX concentrations. (**D**) ALP staining was carried out after 7 days of 10^{-6} M DEX treatment using a BCIP/NBT kit (Scale bar = 100 μm). (**E**) ARS was performed to stain mineralized nodules after 21 days of 10^{-6} M DEX treatment (Scale bar = 100 μm). (**F**) Quantitative assessment of ALP staining intensity. (**G**) Quantitative assessment of ARS intensity. ***$p < 0.001$, **$p < 0.01$, *$p < 0.05$, $n = 3$, relative to controls without DEX.
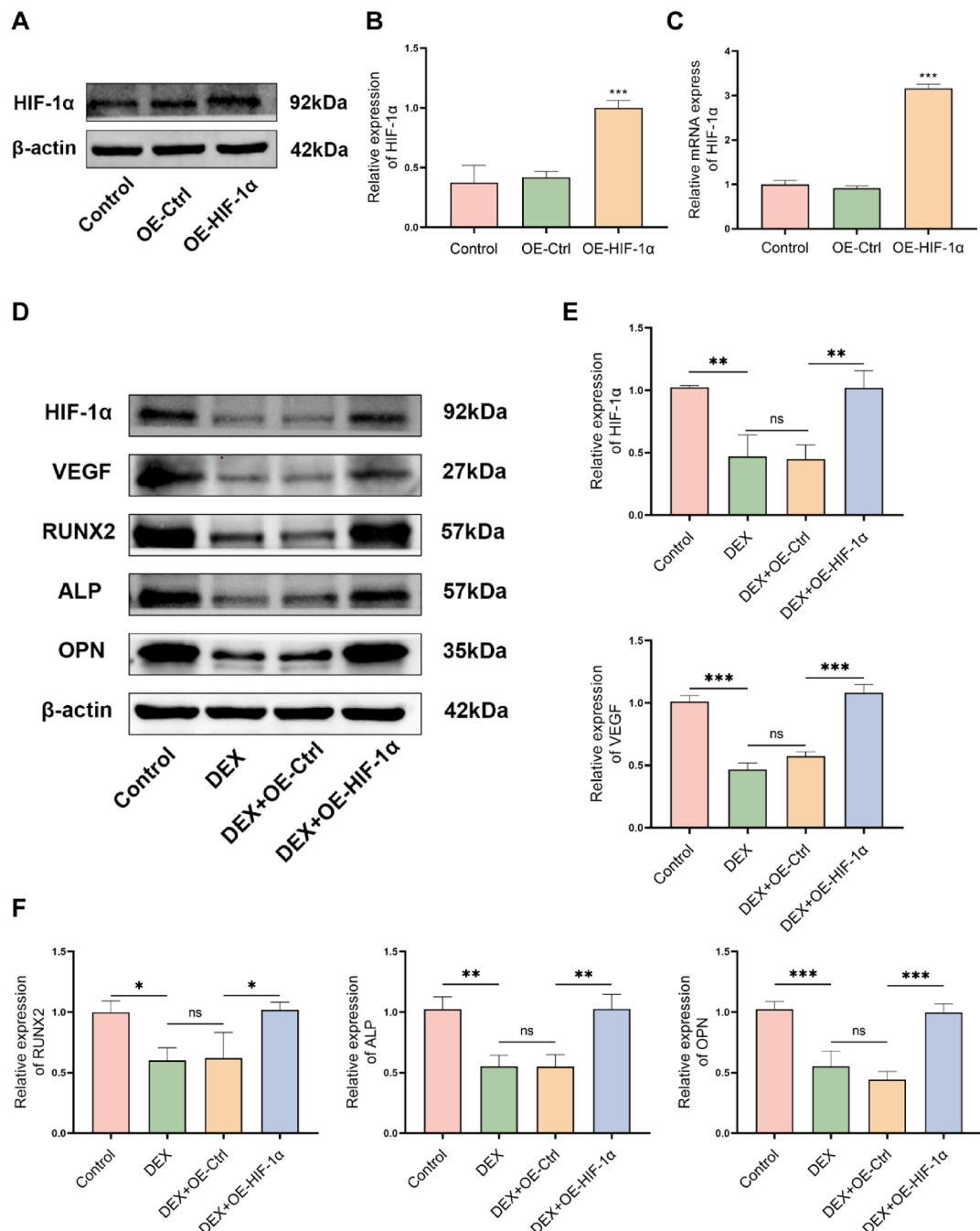
Fig. 3. Assessment of the transfection efficiency of HIF-1α-OE and its effect on the HIF-1α/VEGF signaling pathway, as well as the osteogenic differentiation in DEX-induced MC3T3-E1 cells. **(A)** HIF-1α protein levels in HIF-1α-OE cells were measured *via* WB. **(B)** Quantitative assessment of HIF-1α levels. **(C)** RT-PCR analysis of HIF-1α mRNA levels. **(D)** WB analysis of VEGF, Runx2, HIF-1α, ALP, and OPN protein levels in DEX-treated and HIF-1α overexpressing MC3T3-E1 cells, respectively. **(E)** Statistical analysis of protein expression of HIF-1α, VEGF pathway in DEX-treated and HIF-1α overexpressing MC3T3-E1 cells, respectively. **(F)** Statistical analysis of the protein expression of osteogenic markers, Runx2, ALP, and OPN, in DEX-treated and HIF-1α overexpressing MC3T3-E1 cells, respectively. "ns" stands for "no significant difference," $***p < 0.001$, $**p < 0.01$, $*p < 0.05$, $n = 3$.
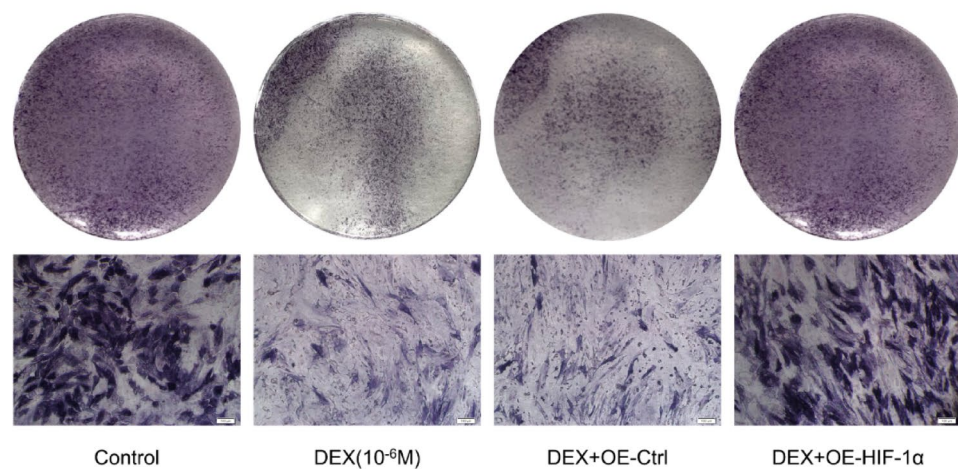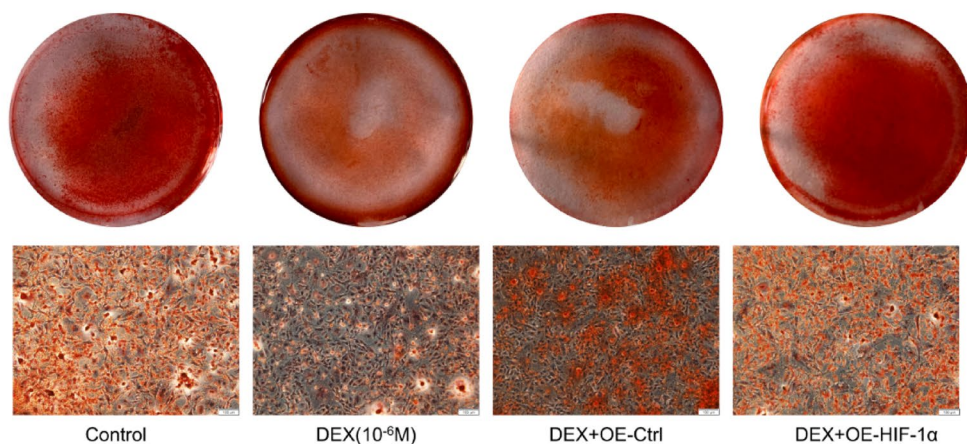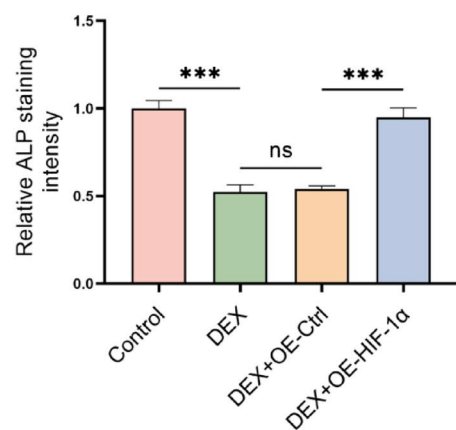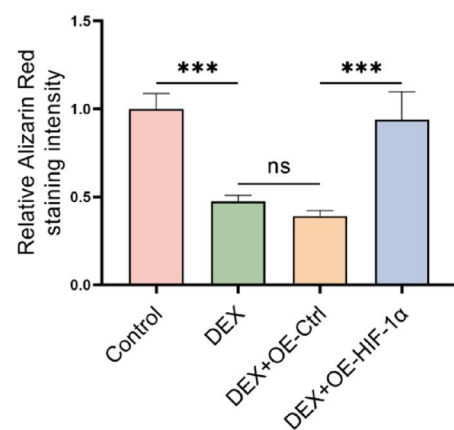
Fig. 4. Effect of HIF-1α-OE on DEX-induced osteogenic staining of MC3T3-E1 cells in vitro. (A) ALP activity was measured *via* ALP staining (Scale bar = 100 μm). (B) Calcified nodules were observed *via* ARS (Scale bar = 100 μm). (C) Quantitative assessment of ALP staining intensity. (D) Quantitative assessment of ARS intensity. "ns" stands for "no significant difference," ***$p < 0.001$, **$p < 0.01$, *$p < 0.05$, $n = 3$.
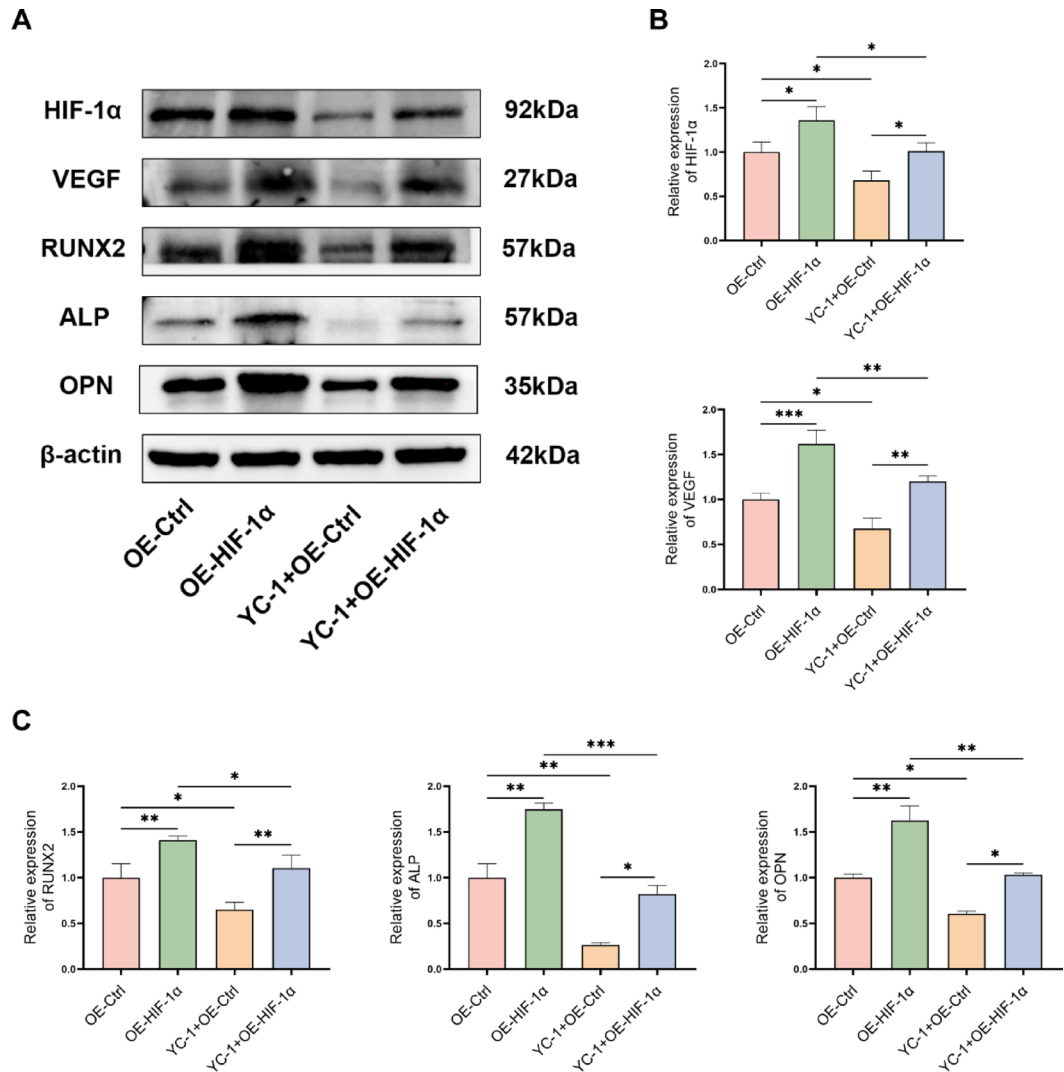
Fig. 5. In DEX-treated MC3T3-E1 cells, HIF-1α inhibitor reversed HIF-1α's protective effect on DEX-induced osteogenic inhibition. **(A)** WB analysis of VEGF, Runx2, HIF-1α, ALP, and OPN protein levels in YC-1-treated and HIF-1α overexpressing MC3T3-E1 cells, respectively. **(B)** Statistical analysis of protein expression of HIF-1α, VEGF pathway in YC-1-treated and HIF-1α overexpressing MC3T3-E1 cells. **(C)** Statistical analysis of Runx2, ALP, and OPN osteogenic marker protein expression in YC-1-treated and HIF-1α overexpressing MC3T3-E1 cells. $***p < 0.001$, $**p < 0.01$, $*p < 0.05$, $n = 3$.

Discussion

SONFH is a severe and irreversible orthopedic condition that significantly reduces the quality of life and increases economic strain on society. SONFH pathogenesis has been explain by several hypotheses, such as aberrant differentiation of BMSCs[35–37], elevated intraosseous pressure[38], adipocyte population[39], fat embolism[40], vascular thrombosis[41], osteoblast or osteocyte apoptosis[42], and oxidative stress[43]. However, its exact pathogenesis remains undetermined. Several studies have indicated that DEX negatively affects osteoblasts, osteocytes, and endothelial cells in vitro; however, its specific mechanism of action in femoral head hormonal osteonecrosis remains elusive. This study indicated an association between reduced HIF-1α expression and DEX-induced osteogenic suppression in osteoblasts. Moreover, DEX inhibited osteoblasts' osteogenic differentiation *via* the HIF-1α/VEGF signaling pathway. The acquired findings offer novel perspectives on the pathogenesis of hormonal femoral head osteonecrosis, providing the basis for the development of more efficient preventive and treatment strategies.

DEX is a synthetic glucocorticoid commonly employed clinically to inhibit bone formation. It has been observed that High DEX doses ($> 10 – 7$ M) markedly inhibit osteoblasts' mineralization ability and osteogenic differentiation[44–46]. The inhibition of osteoblast proliferation and differentiation is crucial for glucocorticoid-induced bone loss[45,47]. Previous literature validates that glucocorticoids suppress HIF-1α protein levels[48]. Here, it was found that DEX-treated MC3T3-E1 cells had reduced HIF-1α and VEGF expression. Moreover, the levels of key osteogenic proteins, including ALP, RUNX2, and OPN, were also reduced. ALP is a glycoprotein that forms homodimers and is produced by osteoblasts during the initial bone formation phases. It is essential for
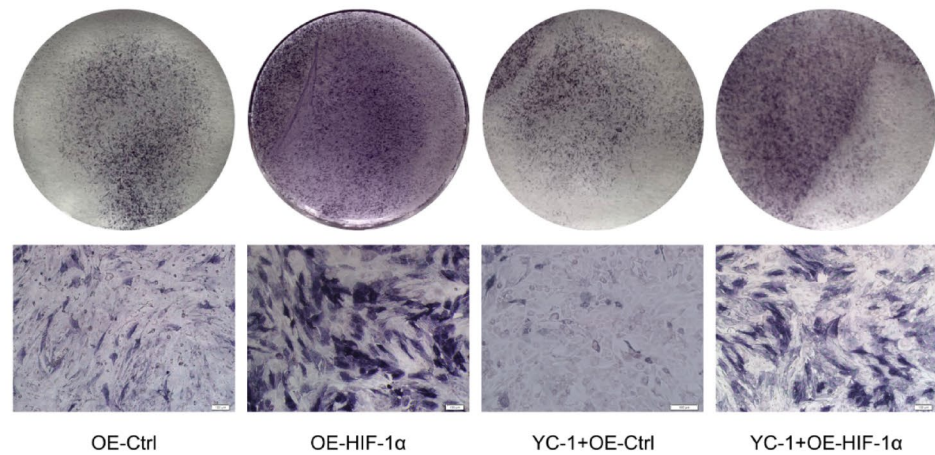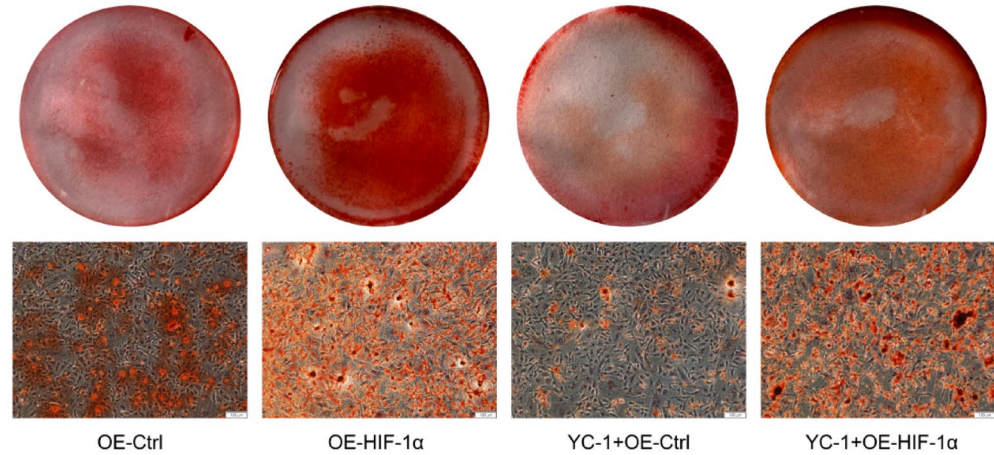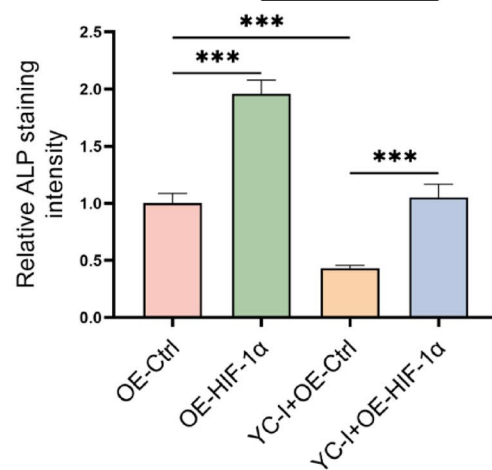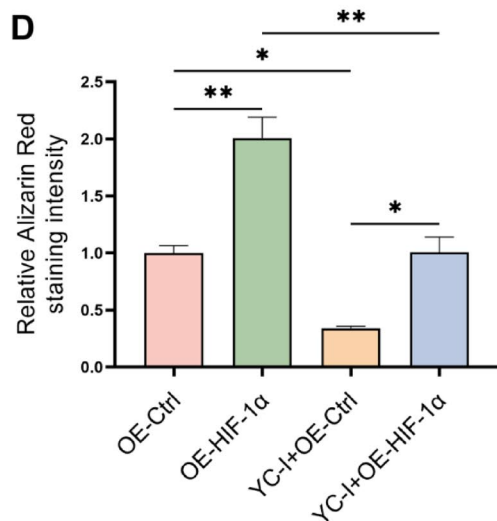
Fig. 6. In DEX-stimulated MC3T3-E1 cells, HIF-1α inhibitor reversed HIF-1α's protection against osteogenic suppression. **(A)** ALP activity was evaluated *via* ALP staining (Scale bar = 100 μm). **(B)** Calcified nodules were detected *via* ARS (Scale bar = 100 μm). **(C)** Quantitative analysis of ALP staining intensity. **(D)** Quantitative assessment of ARS intensity. *$***p < 0.001$, $**p < 0.01$, $*p < 0.05$, n = 3.*
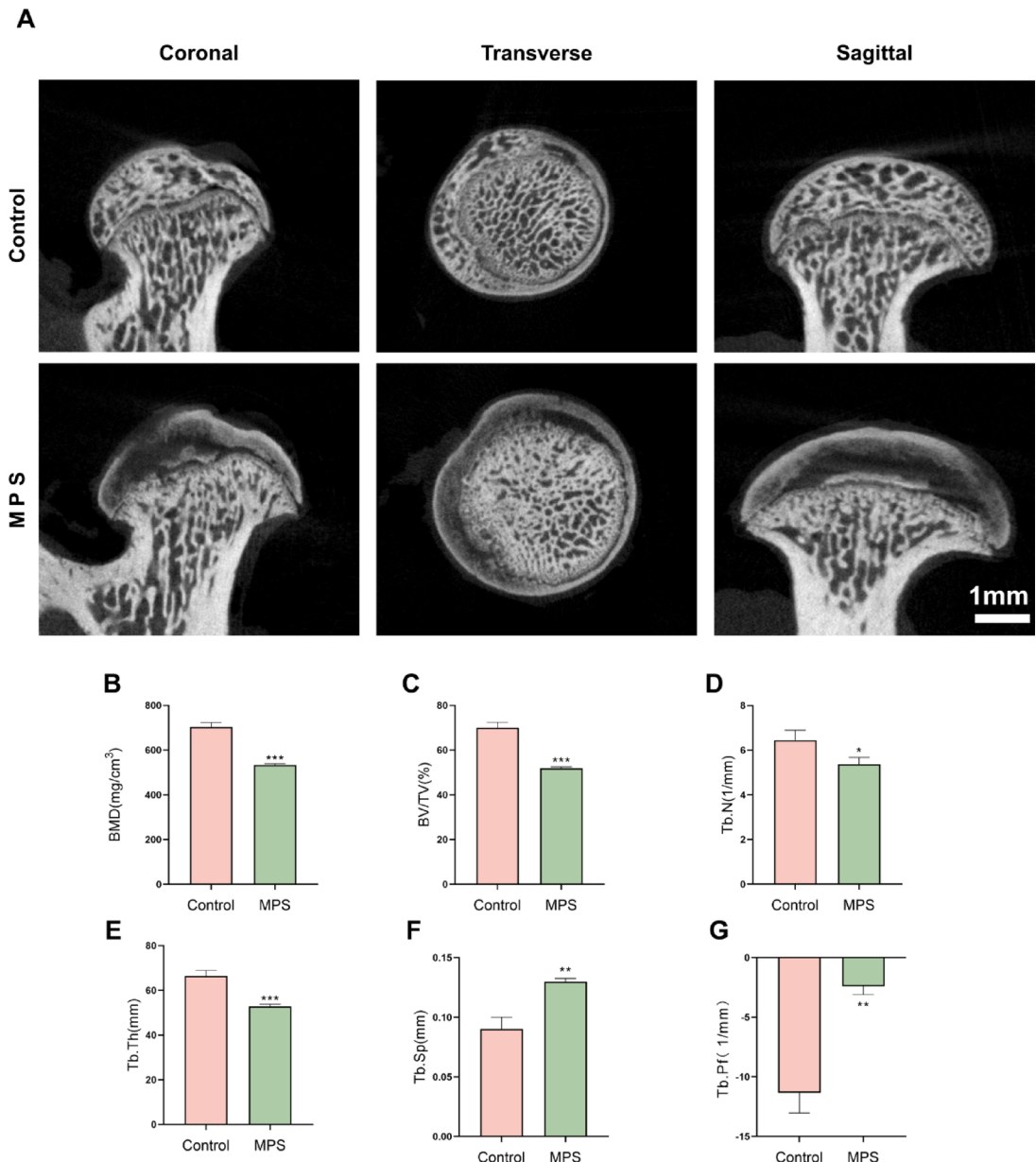
Fig. 7. MicroCT analysis of rat femoral head. **(A)** Micro-CT scans of normal and MPS rats' femoral head and reconstruction of three planar images of the femoral head in coronal, sagittal, and transverse views (Scale bar = 1 mm). **(B-G)** Micro-CT scans of normal and MPS rats' femoral heads. The quantitative assessment of **(B)** BMD, **(C)** BV/TV, **(D)** Tb.N, **(E)** Tb.Th, **(F)** Tb.Sp, and **(G)** Tb.pf in the two groups. *** $p < 0.001$, ** $p < 0.01$, * $p < 0.05$, $n = 3$.

phosphatase breakdown, promoting mineralization, and counteracting osteocalcin's inhibitory influence on bone mineral deposition[49]. Furthermore, ALP levels indicate cell differentiation degree and are often used as an early osteogenic differentiation degree index. OPN is a phosphorylated sulfated glycoprotein that efficiently adsorbs hydroxyapatite, directs mineralization, promotes bone formation, and is an osteoblast differentiation index[50]. RUNX2 is a transcription factor crucial for osteoblast differentiation[51]. Therefore, it was hypothesized that glucocorticoids may promote the development of femoral head necrosis by inhibiting the HIF-1α/VEGF pathway, which in turn inhibits osteoblast'sosteoblasts' osteogenic differentiation. DEX can inhibit osteoblasts and is employed to establish a cellular model of glucocorticoid-induced femoral head necrosis. Successful establishment of the model was indicated by a substantially reduced osteoblast viability[52]. This study indicated a marked decline in MC3T3-E1 cell viability after treatment with 10^{-6} M DEX. Therefore, it was hypothesized that 10^{-6} M DEX has a detrimental effect on MC3T3-E1 cells, and it can modulate osteoblast proliferation and osteogenic differentiation. This indicates that high dosages and prolonged use of DEX might trigger femoral head necrosis and other maladies. Therefore, 10^{-6} M DEX concentration was selected as the treatment dose for MC3T3-E1 cells for subsequent analyses.
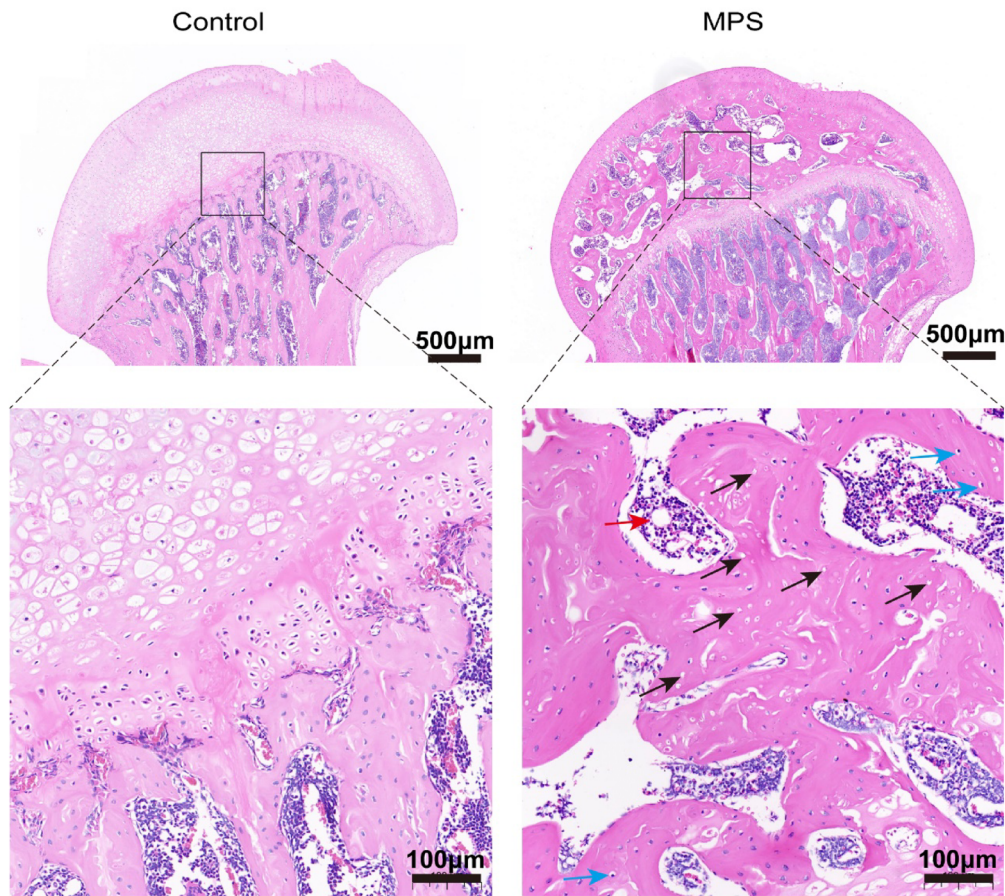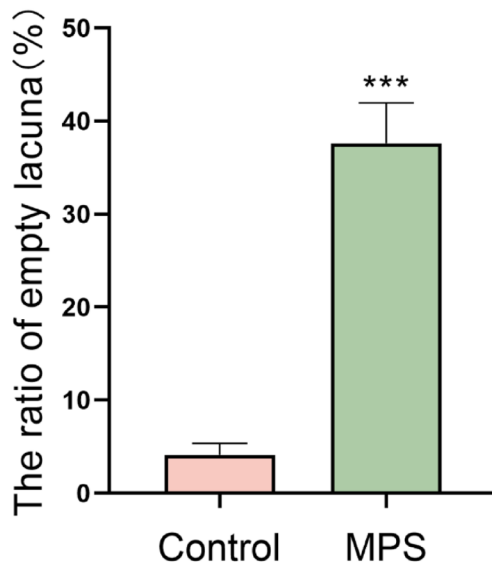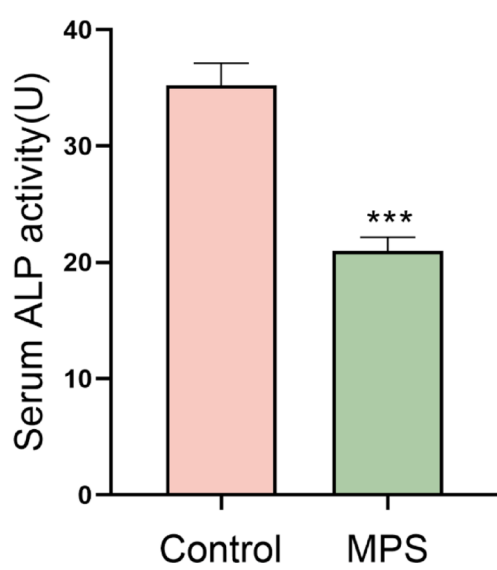
Fig. 8. Schematic of HE-stained rat femoral head and the analysis of serum ALP levels. **(A)** Schematic diagram of HE staining of the femoral head of each group of rats. The black arrows indicate empty bone sockets, the blue arrows indicate nuclear pyknosis, and the red arrows indicate fat droplets. (Scale bar = 500 and 100 μm). **(B)** The ratio of empty lacuna within the femoral head in various groups. **(C)** Serum ALP levels of rats in each group. ***$p < 0.001$, n = 3.
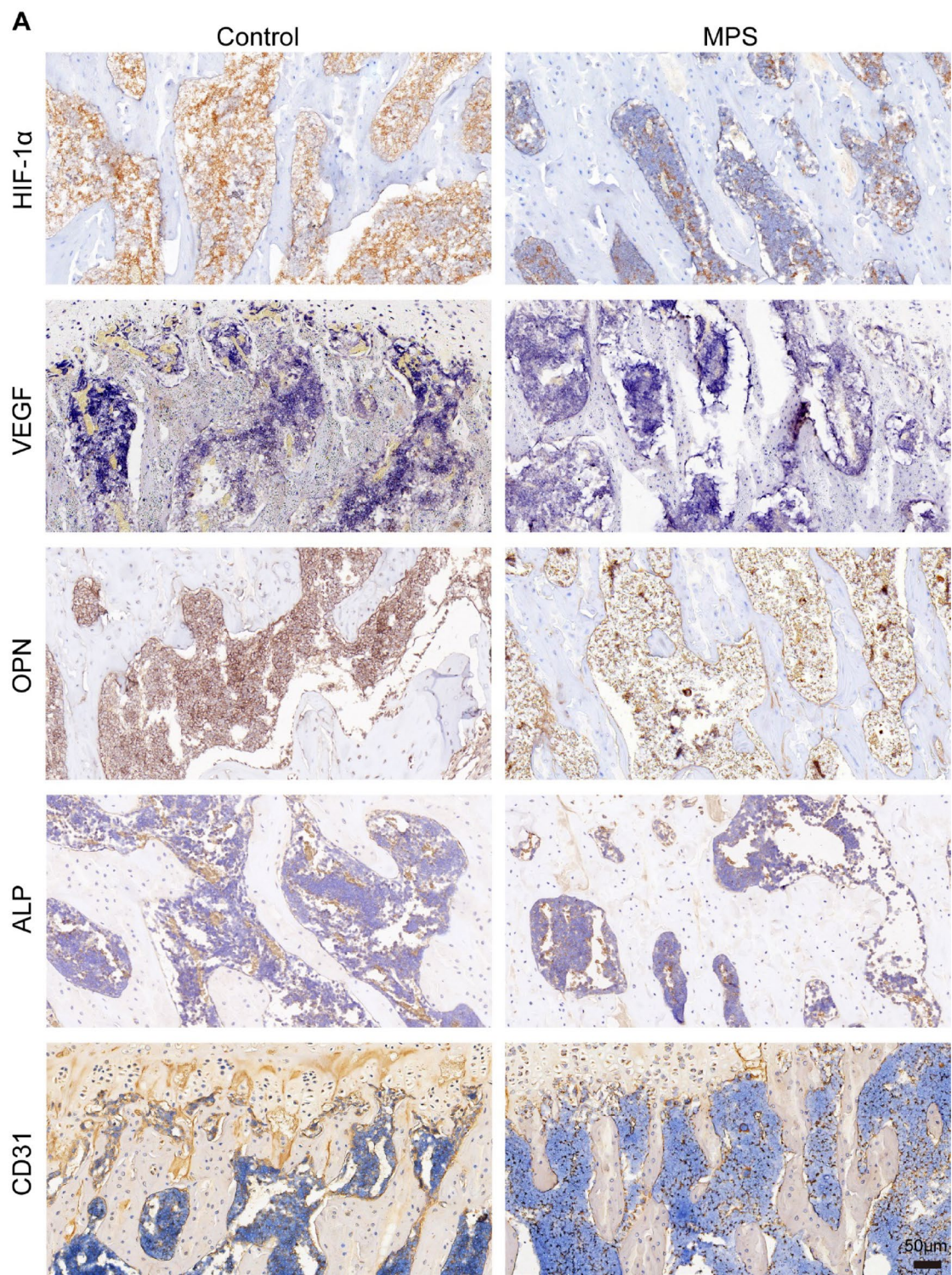
Fig. 9. Immunohistochemical staining and semi-quantitative analysis of rat femoral head. **(A)** Immunohistochemical staining of HIF-1α, VEGF, OPN, ALP, and CD31 in rat femoral head samples from each group. **(B)** Immunohistochemical semi-quantitative analysis of HIF-1α, VEGF, OPN, ALP, and CD31 proteins in rats from each group. $**p < 0.01$, $n = 3$.

It has been indicated that after fracture, HIF-1α increases angiogenesis and bone repair *via* VEGF regulation. Zhang et al. showed that HIF-1α participated in cord MSC-derived exosomes, which induces VEGF expression and fracture repair[53]. Recent studies have indicated that the role of HIF-1α in chondrocytes during tissue repair aids bone recovery. Furthermore, partial HIF-1α deficiency in chondrocytes promotes chondrogenesis and bone healing process by modulating the formation of blood vessels, osteoblasts, and osteoclasts during repair and

B
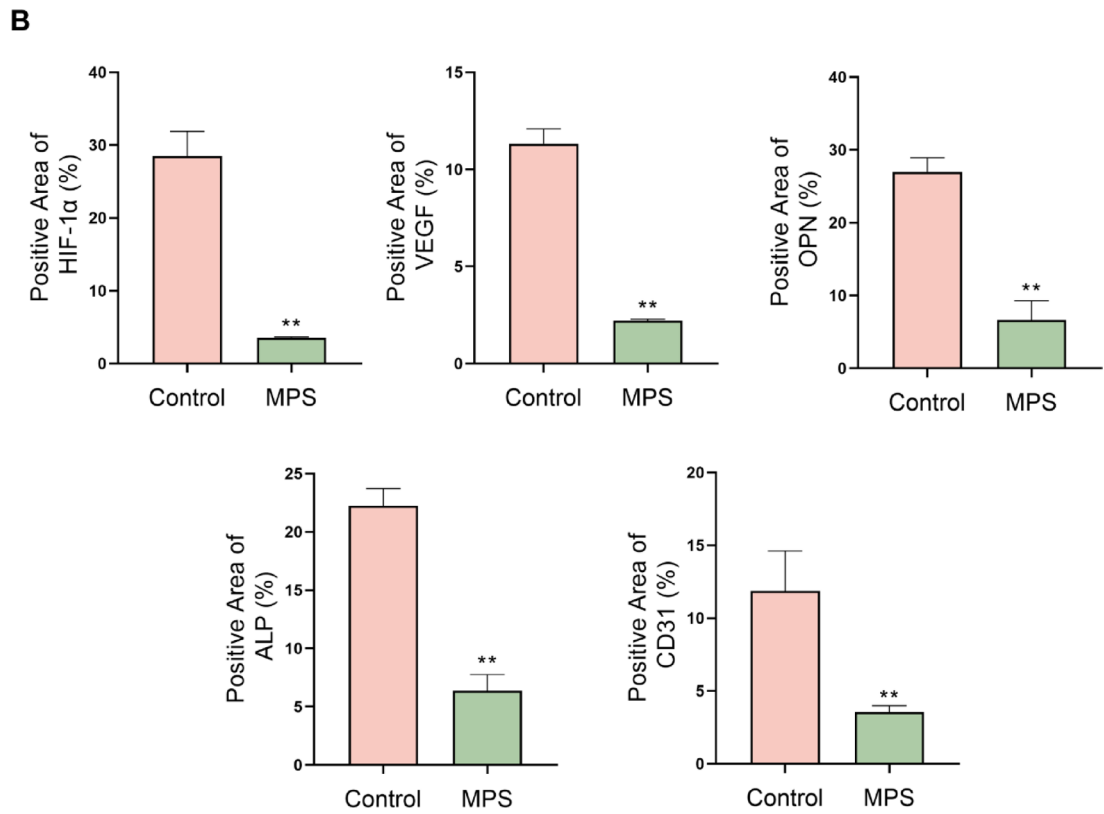
Fig. 9. (continued)

remodeling[54]. Ding et al. revealed that dimethylglycine oxalate increases HIF-1α expression to promote BMSCs' angiogenic activity, which increases bone healing[55]. Here, it was found that HIF-1α-OE reduced the effect of DEX on the osteogenic marker proteins RUNX2, ALP, and OPN in MC3T3-E1 cells by upregulating VEGF. Moreover, ALP staining and ARS results were consistent with these data, indicating that HIF-1α-OE attenuates DEX-mediated suppression of osteogenic differentiation. Moreover, the treatment with YC-1, a HIF-1α inhibitor, substantially inhibited VEGF, RUNX2, ALP, and OPN expression. HIF-1α-OE partially reversed YC-1's inhibitory impact on HIF-1α protein manifestation and VEGF levels. Furthermore, HIF-1α-OE ameliorated the reduction in VEGF expression, whereas HIF-1α inhibition reduced VEGF expression. Altogether, it is suggested that DEX inhibits osteoblasts' osteogenic differentiation *via* the signaling pathway of HIF-1α/VEGF.

Here, the successful establishment of the hormonal femoral head necrosis model was confirmed by the Micro-CT and HE staining. Furthermore, the diagnosis of osteonecrosis was confirmed by histopathological observation of empty cavities or nuclear pyknosis of bone cells in the trabecular bone, accompanied by necrosis of surrounding bone marrow cells. Currently, Micro-CT is the most efficient detection system for the quantitative evaluation of bone microstructure. In this study, Micro-CT scanning was performed to analyze the changes of bone trabeculae in the femoral head. The SONFH rats indicated significantly more subchondral bone cavities, femoral head collapse, and increased Tb.Sp and Tb.Pf, as well as reduced Tb.N, Tb.Th, and BV/TV in contrast to normal Ctrl rats, consistent with a previous study[56]. The HE staining results revealed that, in addition to the altered bone trabeculae morphology, there were numerous vacant bone sockets in the subchondral region of the model group. Combined with the respective quantitative scoring results, the rat SONFH model was established.

The in-vivo findings indicated HIF-1α expression in both the SONFH model and Ctrl groups. The findings indicated that the expression of HIF-1α was lower in the model group relative to the Ctrl group. This was validated by Zhang et al., who indicated that BMMSCs infected with Lentivirus encoding HIF-1α (Lenti-HIF-1α) significantly increased the production of HIF-1α protein. Furthermore, implantation of BMMSCs overexpressing HIF-1α into femoral heads of SOFH mice significantly reduced osteonecrotic areas and enhanced bone repair, thus preserving the structural integrity of femoral heads[57]. Overall, these results suggest that HIF-1α plays a key role in the pathogenesis of SONFH. The literature has indicated increased osteocyte death and osteoclast formation in necrotic areas in osteonecrosis, but with reduced vascularization and impaired osteogenic activity. The present study revealed significantly impaired staining of OPN, ALP, VEGF, and CD31 in the necrotic region. Furthermore, serum ALP levels were assessed to determine the presence and degree of osteoblast differentiation. Moreover, serum ALP assays showed markedly reduced in vivo ALP activity in the model group relative to the Ctrl group.

The results of this study are consistent with previous studies[58], further confirming the key role of HIF-1α in femoral head necrosis. These factors are, therefore, considered major regulators of or correlate with the osteogenic differentiation process[59,60]. Osteoblasts are mainly derived from BMSCs, which first undergo

spectral differentiation and become preosteoblasts. Glucocorticoid inhibits preosteoblast differentiation and maturation by suppressing the expression of Runx2, which subsequently reduces ALP and OPN levels[61]. The in vivo results indicated an association of HIF-1α expression with OPN and ALP expression, which suggested that DEX reduces osteoblasts' osteogenic differentiation by inhibiting the HIF-1α/VEGF signaling pathway. VEGF is crucial for promoting neointimal development and increasing vascular permeability[62]. Relative to the Ctrl group, a substantial decrease was observed in HIF-1α, VEGF, and CD31 levels in the MPS-treated group. This might be because DEX promotes the onset of femoral head necrosis by suppressing the HIF-1α/VEGF signaling pathway, thus delaying angiogenesis. The precise mechanism of this regulation requires further investigation and is a focus of our future research.

Although this study validates that DEX inhibits osteoblast differentiation through the HIF-1α/VEGF signaling pathway, the specific mechanism by which DEX regulates HIF-1α expression warrants further research. Jiang et al. found that low-dose DEX reduced small ubiquitin-like modifications of HIF-1α and Oct4, increased their degradation, and inhibited their translocation from the cytoplasm to the nucleus, thereby reducing their accumulation and stable nuclear expression, ultimately reducing hypoxia tolerance and stem cell maintenance potential[63]. Gao et al.. reported that prenatal DEX exposure induced high methylation of the bone morphogenetic protein 4 promoter DNA in cardiomyocytes, significantly reducing the binding activity of cardiac ischemia-induced transcription factor HIF-1α[64].

Several studies have indicated that the inhibitory effect of DEX on HIF-1α is closely related to the glucocorticoid receptor (GR). Xu et al.[65] showed that GR antagonist (RU486 and DEX) treated MC3T3-E1 cells had increased HIF-1α expression, suggesting glucocorticoids reduce HIF-1α expression levels by binding to GR. Under hypoxic conditions, HIF-1-dependent gene expression is further upregulated by glucocorticoids *via* GR[66]. This upregulation cannot be replaced by other steroid receptors and is thought to result from the interaction between GR and HIF-1α's transcriptional activation domain. Glucocorticoid-bound GR transactivates TSC22D3 *via* glucocorticoid response element (GRE), causing ubiquitin-proteasome system (UPS)-mediated degradation of HIF-1α, which is otherwise stabilized by hypoxia and diabetes for the induction of Müller glial galectin-1 expression[67]. Anna et al. performed in vivo and in vitro assays and identified that the GR signaling pathway reduced the activity of HIF-1α on the VEGFA promoter, leading to decreased VEGFA expression[68]. However, the absence of GRE consensus sites in Hif-1α promoter suggests a more complex level of regulation by the GC/GR pathway[69]. Alternative mechanisms, such as potential crosstalk between GR and PPARγ, could be considered to modulate the HIF-1α/VEGFA pathway and therefore AT angiogenesis[70].

Currently, there is a lack of direct research on how the HIF-1α/VEGF axis regulates the osteogenic differentiation marker RUNX2. Zhang et al. found that BMMSC-Exos transplantation induces a critical effect on the treatment of nonunion by promoting osteogenesis and angiogenesis[71]. This promoting effect might be ascribed to the activation of the BMP-2/Smad1/RUNX2 and the HIF-1α/VEGF signaling pathways. Shan et al. suggest that astragaloside IV can promote osteogenesis and angiogenesis through the Akt/Runx2 and Akt/HIF-1α/VEGF pathways, respectively, thereby preventing SONFH[72]. Moreover, it can also inhibit apoptosis and oxidative stress through the Akt/Bad/Bcl-2 and Akt/Nrf2/HO-1 pathways, respectively. Tian et al. indicated that whole-body vibration therapy upregulates Piezo1 to promote osteogenic differentiation, potentially by enhancing the HIF-1α/VEGF axis and regulating H-vessel angiogenesis by activating Piezo1 ion channel[73]. This mechanism may improve blood flow supply and enhance osteogenic differentiation within the femoral head. Overall, these studies indicate that the HIF-1α/VEGF signaling pathway is closely related to angiogenesis. However, there are currently no reports on how the HIF-1α/VEGF axis regulates RUNX2, which warrants further research.

Limitations

This study provides evidence that the HIF-1α/VEGF signaling pathway is associated with SONFH pathogenesis through ex vivo experiments; however, this study has certain limitations. This study only studied the role of the HIF-1α/VEGF signaling pathway in glucocorticoid-induced osteogenic inhibition of osteoblasts due to the close temporal and spatial correlation between angiogenesis and osteogenesis. Further research is warranted to understand this signaling pathway's role in SONFH angiogenesis.

Conclusion

In summary, it was observed that glucocorticoids can inhibit osteoblasts' osteogenic differentiation by activating the HIF-1α/VEGF signaling pathway, which contributes to SONFH progression. The above findings offer novel perspectives for comprehensively understanding the molecular mechanism underlying the osteogenic inhibition of osteoblasts triggered by glucocorticoids. Overall, selective HIF-1α-OE could potentially be employed to mitigate glucocorticoid-induced osteonecrosis of the femoral head.

Data availability

The datasets used and analysed during the current study are available from the corresponding author on reasonable request.

References

1. Smolen, J. S. et al. EULAR recommendations for the management of rheumatoid arthritis with synthetic and biological disease-modifying antirheumatic drugs: 2022 update. *Ann. Rheum. Dis.* **82** (1), 3–18 (2023).
2. Hellmich, B. et al. EULAR recommendations for the management of ANCA-associated vasculitis: 2022 update. *Ann. Rheum. Dis.* **83** (1), 30–47 (2024).

3. Teschke, R. Treatment of Drug-Induced liver injury. *Biomedicines* **11** (1), 15 (2022).
4. Ding, Z. & Huang, H. Mesenchymal stem cells in rabbit meniscus and bone marrow exhibit a similar feature but a heterogeneous multi-differentiation potential: superiority of meniscus as a cell source for meniscus repair. *BMC Musculoskelet. Disord.* **16**, 65 (2015).
5. Han, L. et al. The shift in the balance between osteoblastogenesis and adipogenesis of mesenchymal stem cells mediated by glucocorticoid receptor. *Stem Cell Res. Ther.* **10** (1), 377 (2019).
6. Ding, P., Zhang, W., Tan, Q., Yao, C. & Lin, S. Impairment of Circulating endothelial progenitor cells (EPCs) in patients with glucocorticoid-induced avascular necrosis of the femoral head and changes of EPCs after glucocorticoid treatment in vitro. *J. Orthop. Surg, Res.* **14** (1), 226 (2019).
7. Chang, C., Greenspan, A. & Gershwin, M. E. The pathogenesis, diagnosis and clinical manifestations of steroid-induced osteonecrosis. *J. Autoimmun.* **110**, 102460 (2020).
8. Yoon, B-H. et al. Etiologic classification criteria of ARCO on femoral head osteonecrosis part 1: Glucocorticoid-Associated osteonecrosis. *J. Arthroplast.* **34** (1), 163–168e1 (2019).
9. Zhang, S-Y., Wang, F., Zeng, X-J., Huang, Z. & Dong, K-F. Astragalus polysaccharide ameliorates steroid-induced osteonecrosis of femoral head through miR-206/HIF-1α/BNIP3 axis. *Kaohsiung J. Med. Sci.* **37** (12), 1089–1100 (2021).
10. Duan, L. et al. Magnetic targeting of HU-MSCs in the treatment of Glucocorticoid-Associated osteonecrosis of the femoral head through Akt/Bcl2/Bad/Caspase-3 pathway. *Int. J. Nanomed.* **15**, 3605–3620 (2020).
11. Migliorini, F. et al. Operative management of avascular necrosis of the femoral head in skeletally immature patients: A systematic review. *Life (Basel Switzerland).* **12** (2), 179 (2022).
12. Sadile, F., Bernasconi, A., Russo, S. & Maffulli, N. Core decompression versus other joint preserving treatments for osteonecrosis of the femoral head: a meta-analysis. *Br. Med. Bull.* **118** (1), 33–49 (2016).
13. Quaranta, M., Miranda, L., Oliva, F., Aletto, C. & Maffulli, N. Osteotomies for avascular necrosis of the femoral head. *Br. Med. Bull.* **137** (1), 98–111 (2021).
14. Migliorini, F., Maffulli, N., Eschweiler, J., Tingart, M. & Baroncini, A. Core decompression isolated or combined with bone Marrow-Derived cell therapies for femoral head osteonecrosis. *Expert Opin. Biol. Ther.***21**(3), 423–430 (2021).
15. Migliorini, F. et al. Prognostic factors in the management of osteonecrosis of the femoral head: A systematic review. *Surgeon: J. Royal Colleges Surg. Edinb. Irel.* **21** (2), 85–98 (2023).
16. Qin, Q. et al. Hypoxia-Inducible factors signaling in osteogenesis and skeletal repair. *Int. J. Mol. Sci.* **23** (19), 11201 (2022).
17. Tao, J. et al. Spatiotemporal correlation between HIF-1α and bone regeneration. *FASEB Journal: Official Publication Federation Am. Soc. Experimental Biology*. **36** (10), e22520 (2022).
18. Archacka, K. et al. Hypoxia preconditioned bone marrow-derived mesenchymal stromal/stem cells enhance myoblast fusion and skeletal muscle regeneration. *Stem Cell Res. Ther.* **12** (1), 448 (2021).
19. Zhou, B. et al. Dimethyloxalyl Glycine regulates the HIF-1 signaling pathway in mesenchymal stem cells. *Stem Cell. Reviews Rep.* **16** (4), 702–710 (2020).
20. Costa, M. H. G. et al. Dimethyloxalylglycine, a small molecule, synergistically increases the homing and angiogenic properties of human mesenchymal stromal cells when cultured as 3D spheroids. *Biotechnol. J.* **16** (5), e2000389 (2021).
21. Ghadge, S. et al. Abstract 16652: Inhibition of Prolyl hydroxylase as a novel therapeutic target for Hif-Mediated Sdf-1 activation and stem cell homing in the ischemic heart. *Circulation* **128** (suppl_22), A16652–A16652 (2013).
22. Semenza, G. L. HIF-1 and mechanisms of hypoxia sensing. *Curr. Opin. Cell Biol.* **13** (2), 167–171 (2001).
23. Yang, C. et al. HIF-1: structure, biology and natural modulators. *Chin. J. Nat. Med.* **19** (7), 521–527 (2021).
24. Chen, W. et al. HIF-1α regulates bone homeostasis and angiogenesis, participating in the occurrence of bone metabolic diseases. *Cells* **11** (22), 3552 (2022).
25. Regan, J. N. et al. Up-regulation of glycolytic metabolism is required for HIF1α-driven bone formation. *Proc. Natl. Acad. Sci. U.S.A.* **111** (23), 8673–8678 (2014).
26. Liu, W. et al. Hypoxic mesenchymal stem cell-derived exosomes promote bone fracture healing by the transfer of miR-126. *Acta Biomater.* **103**, 196–212 (2020).
27. Jahangir, S., Hosseini, S., Mostafaei, F., Sayahpour, F. A. & Baghaban Eslaminejad, M. 3D-porous β-tricalcium phosphate-alginate-gelatin scaffold with DMOG delivery promotes angiogenesis and bone formation in rat calvarial defects. *J. Mater. Sci.: Mater. Med.* **30** (1), 1 (2018).
28. Yin, X. et al. Oxygen tension regulating hydrogels for vascularization and osteogenesis via sequential activation of HIF-1α and ERK1/2 signaling pathways in bone regeneration. *Biomaterials Adv.* **161**, 213893 (2024).
29. Bixel, M. G. et al. Angiogenesis is uncoupled from osteogenesis during calvarial bone regeneration. *Nat. Commun.* **15** (1), 4575 (2024).
30. García-Martín, A., Acitores, A., Maycas, M., Villanueva-Peñacarrillo, M. L. & Esbrit, P. Src kinases mediate VEGFR2 transactivation by the osteostatin domain of PTHrP to modulate osteoblastic function. *J. Cell. Biochem.* **114** (6), 1404–1413 (2013).
31. Wu, D., Liu, L., Fu, S. & Zhang, J. Osteostatin improves the osteogenic differentiation of mesenchymal stem cells and enhances angiogenesis through HIF-1α under hypoxia conditions in vitro. *Biochem. Biophys. Res. Commun.* **606**, 100–107 (2022).
32. Watson, E. C. & Adams, R. H. Biology of bone: the vasculature of the skeletal system. *Cold Spring Harbor Perspect. Med.* **8** (7), a031559 (2018).
33. Yang, N. et al. Inhibition of MAGL activates the Keap1/Nrf2 pathway to attenuate glucocorticoid-induced osteonecrosis of the femoral head. *Clin. Translational Med.* **11** (6), e447 (2021).
34. Xu, H. et al. Jintiange capsule ameliorates glucocorticoid-induced osteonecrosis of the femoral head in rats by regulating the activity and differentiation of BMSCs. *J. Traditional Complement. Med.* **14** (5), 568–580 (2024).
35. Gong, L-L. et al. Genetic risk factors for glucocorticoid-induced osteonecrosis: a meta-analysis. *Steroids* **78** (4), 401–408 (2013).
36. Weinstein, R. S. Glucocorticoid-induced osteonecrosis. *Endocrine* **41** (2), 183–190 (2012).
37. Kerachian, M. A., Séguin, C. & Harvey, E. J. Glucocorticoids in osteonecrosis of the femoral head: a new Understanding of the mechanisms of action. *J. Steroid Biochem. Mol. Biol.* **114** (3–5), 121–128 (2009).
38. Hungerford, D. S. & Lennox, D. W. The importance of increased intraosseous pressure in the development of osteonecrosis of the femoral head: implications for treatment. *Qld. Gov. Min. J.* **16** (4), 635–654 (1985).
39. Miyanishi, K. et al. Bone marrow fat cell enlargement and a rise in intraosseous pressure in steroid-treated rabbits with osteonecrosis. *Bone* **30** (1), 185–190 (2002).
40. Zhang, Q. & Jin, L. V. J. Role of coagulopathy in glucocorticoid-induced osteonecrosis of the femoral head. *J. Int. Med. Res.* **46** (6), 2141–2148 (2018).
41. Rezus, E. et al. Osteonecrosis of the femoral head in patients with Hypercoagulability-From pathophysiology to therapeutic implications. *Int. J. Mol. Sci.* **22** (13), 6801 (2021).
42. Deng, S. et al. Dexamethasone induces osteoblast apoptosis through ROS-PI3K/AKT/GSK3β signaling pathway. Biomedicine & Pharmacotherapy = Biomedecine & Pharmacotherapie. ;110:602–608. (2019).
43. Kubo, Y. et al. Adverse effects of oxidative stress on bone and vasculature in Corticosteroid-Associated osteonecrosis: potential role of nuclear factor erythroid 2-Related factor 2 in cytoprotection. *Antioxid. Redox. Signal.* **35** (5), 357–376 (2021).
44. Yu, W., Zhu, C., Xu, W., Jiang, L. & Jiang, S. Neuropeptide Y1 receptor regulates Glucocorticoid-Induced Inhibition of osteoblast differentiation in murine MC3T3-E1 cells via ERK signaling. *Int. J. Mol. Sci.* **17** (12), 2150 (2016).

45. Rauch, A. et al. Glucocorticoids suppress bone formation by attenuating osteoblast differentiation via the monomeric glucocorticoid receptor. *Cell Metabol.* **11** (6), 517–531 (2010).

46. Xu, S. et al. Dexamethasone interferes with osteoblasts formation during osteogenesis through altering IGF-1-mediated angiogenesis. *J. Cell. Physiol.* **234** (9), 15167–15181 (2019).

47. Migliaccio, S. et al. Glucocorticoid-induced osteoporosis: an osteoblastic disease. *Aging Clin. Exp. Res.* **19** (3 Suppl), 5–10 (2007).

48. Weinstein, R. S. et al. Endogenous glucocorticoids decrease skeletal angiogenesis, vascularity, hydration, and strength in aged mice. *Aging Cell.* **9** (2), 147–161 (2010).

49. Vimalraj, S. Alkaline phosphatase: structure, expression and its function in bone mineralization. *Gene* **754**, 144855 (2020).

50. Icer, M. A. & Gezmen-Karadag, M. The multiple functions and mechanisms of osteopontin. *Clin. Biochem.* **59**, 17–24 (2018).

51. Komori, T. Regulation of proliferation, differentiation and functions of osteoblasts by Runx2. *Int. J. Mol. Sci.* **20** (7), 1694 (2019).

52. Yang, H. et al. Palliative effect of rotating magnetic field on glucocorticoid-induced osteonecrosis of the femoral head in rats by regulating osteoblast differentiation. *Biochem. Biophys. Res. Commun.* **725**, 150265 (2024).

53. Zhang, Y. et al. Exosomes from human umbilical cord mesenchymal stem cells enhance fracture healing through HIF-1α-mediated promotion of angiogenesis in a rat model of stabilized fracture. *Cell Prolif.* **52** (2), e12570 (2019).

54. Hong, C. et al. Partial deficiency of HIF-1α in chondrocytes effected bone repair of mandibular condylar neck. *Arch. Oral Biol.* **122**, 105023 (2021).

55. Ding, H. et al. Dimethyloxaloylglycine improves angiogenic activity of bone marrow stromal cells in the tissue-engineered bone. *Int. J. Biol. Sci.* **10** (7), 746–756 (2014).

56. Chen, K. et al. Steroid-induced osteonecrosis of the femoral head reveals enhanced reactive oxygen species and hyperactive osteoclasts. *Int. J. Biol. Sci.* **16** (11), 1888–1900 (2020).

57. Anon Bone marrow mesenchymal stem cells overexpressing HIF-1α prevented the progression of Glucocorticoid-Induced avascular osteonecrosis of femoral heads in Mice . *Cell Transplantation* **31**, 9636897221082687 (2022).

58. Pang, K., Wang, S., Li, M. & Zhou, Z. Autophagy in femoral head necrosis of broilers bone metabolism parameters and Autophagy-Related gene expression in femoral head necrosis induced by glucocorticoid in broilers. *Front. Veterinary Sci.* **8**, 746087 (2021).

59. Song, S. et al. HIF-1α increases the osteogenic capacity of ADSCs by coupling angiogenesis and osteogenesis via the HIF-1α/VEGF/AKT/mTOR signaling pathway. *J. Nanobiotechnol.* **21** (1), 257 (2023).

60. Ruan, H. et al. Inhibition of Caspase-1-mediated pyroptosis promotes osteogenic differentiation, offering a therapeutic target for osteoporosis. *Int. Immunopharmacol.* ;**124** (Pt B), 110901 (2023).

61. Xie, B. et al. Geniposide alleviates Glucocorticoid-Induced Inhibition of osteogenic differentiation in MC3T3-E1 cells by ERK pathway. *Front. Pharmacol.* **10**, 411 (2019).

62. Apte, R. S., Chen, D. S. & Ferrara, N. VEGF in signaling and disease: beyond discovery and development. *Cell* **176** (6), 1248–1264 (2019).

63. Jiang, Z. et al. Dexamethasone inhibits stemness maintenance and enhances chemosensitivity of hepatocellular carcinoma stem cells by inducing desumoylation of HIF–1α and Oct4. *Int. J. Oncol.* **57** (3), 780–790 (2020).

64. Gao, L-T., Yuan, J-Q., Zhang, Z-Y., Zhao, H-M. & Gao, L. Hypermethylation of the Bmp4 promoter dampens binding of HIF-1α and impairs its cardiac protective effects from oxidative stress in prenatally GC-exposed offspring. *Cell. Mol. Life Sci.* **80** (3), 58 (2023).

65. Xu, W-N., Zheng, H-L., Yang, R-Z., Jiang, L-S. & Jiang, S-D. HIF-1α regulates Glucocorticoid-Induced osteoporosis through PDK1/AKT/mTOR signaling pathway. *Front. Endocrinol.* **10**, 922 (2019).

66. Kodama, T. et al. Role of the glucocorticoid receptor for regulation of hypoxia-dependent gene expression. *J. Biol. Chem.* **278** (35), 33384–33391 (2003).

67. Kanda, A. et al. TSC22D3 attenuates hypoxia- and diabetes-induced Müller glial galectin-1 expression via HIF-1α destabilization. *J. Cell. Mol. Med.* **24** (8), 4589–4599 (2020).

68. Vali, A. et al. Adipocyte glucocorticoid receptor activation with high glucocorticoid doses impairs healthy adipose tissue expansion by repressing angiogenesis. *Diabetes* **73** (2), 211–224 (2023).

69. Minet, E. et al. HIF1A gene transcription is dependent on a core promoter sequence encompassing activating and inhibiting sequences located upstream from the transcription initiation site and Cis elements located within the 5'UTR. *Biochem. Biophys. Res. Commun.* **261** (2), 534–540 (1999).

70. Corvera, S., Solivan-Rivera, J. & Yang Loureiro, Z. Angiogenesis in adipose tissue and obesity. *Angiogenesis* **25** (4), 439–453 (2022).

71. Zhang, L. et al. Exosomes from bone marrow mesenchymal stem cells enhance fracture healing through the promotion of osteogenesis and angiogenesis in a rat model of nonunion. *Stem Cell Res. Ther.* **11** (1), 38 (2020).

72. Shan, H. et al. Effects of Astragaloside IV on glucocorticoid-induced avascular necrosis of the femoral head via regulating Akt-related pathways. *Cell Prolif.* **56** (11), e13485 (2023).

73. Tian, J-Q. et al. Effect of whole body vibration therapy in the rat model of steroid-induced osteonecrosis of the femoral head. *Front. Cell. Dev. Biology.* **11**, 1251634 (2023).

Acknowledgements

Author contributions

HaoXu Tang and Lingli Yuan designed the overall experimental idea, HaoXu Tang, ZhiYan Xu, YingJie Liang, ,and Ce Li performed the experimental manipulation and data collection, GuiFen Jiang, PengLin Ding, and MinLong Qian performed the data analysis, HaoXu Tang, GuiFen Jiang,, and Lingli Yuan wrote and reviewed the article. All authors approved the final manuscript.

Funding

Declarations

Ethics approval and consent to participate

This study was approved by the ethics committee of the Second Affiliated Hospital of Bengbu Medical College (Ethics approval number: No. [2022] 159). All methods were performed in accordance with the relevant guidelines and regulations. Clinical trial number: not applicable.

Competing interests
The authors declare no competing interests.

Additional information
Supplementary Information The online version contains supplementary material available at https://doi.org/10.1038/s41598-025-15018-4.

Correspondence and requests for materials should be addressed to L.Y.

Reprints and permissions information is available at www.nature.com/reprints.

Publisher's note Springer Nature remains neutral with regard to jurisdictional claims in published maps and institutional affiliations.